

Charge injection into the atmosphere by explosive volcanic eruptions through triboelectrification and fragmentation charging

Joshua Méndez Harper^a, Corrado Cimorelli^b, Valeria Cigala^b, Ulrich Kueppers^b, Josef Dufek^a

^a*Department of Earth Science, University of Oregon, Eugene OR, 97403, USA*

^b*Department für Geo- und Umweltwissenschaften, Ludwig-Maximilians-Universität München, Munich BY, 80333, Germany*

Abstract

Volcanic eruptions are associated with a wide range of electrostatic effects. Increasing evidence suggests that high-altitude discharges (lightning) in maturing plumes are driven by electrification processes that require the formation of ice (analogous to processes underpinning meteorological thunderstorms). However, electrical discharges are also common at or near the volcanic vent. A number of “ice-free” electrification mechanisms have been proposed to account for this activity: fractocharging, triboelectric charging, radioactive charging, and charging through induction. Yet, the degree to which each mechanism contributes to a jet’s total electrification and how electrification in the gas-thrust region influences electrostatic processes aloft remains poorly constrained. Here, we use a shock-tube to simulate overpressured volcanic jets capable of producing spark discharges in the absence of ice. These discharges may be representative of the continual radio frequency (CRF) emissions observed at a number of eruptions. Using a suite of electrostatic sensors, we demonstrate the presence of size-dependent bipolar charging (SDBC) in a discharge-bearing flow for the first time. SDBC has been readily associated with triboelectric charging in other contexts and provides direct evidence that contact and frictional electrification play significant roles in electrostatic processes in the vent and near-vent regions of an eruption. Additionally, we find that particles leaving the region where discharges occur remain moderately electrified. This degree of electrification may be sufficient to drive near-vent lightning higher in the column. Thus, near-vent discharges may be underpinned by the same electrification mechanisms driving CRF,

albeit involving greater degrees of charge separation.

Keywords: Tribocharging, Volcanic lightning, Size-dependent bipolar charging

1. Introduction

1.1. Plume lightning and proximal discharges

Investigations over the last two decades reveal that electrical activity in volcanic columns may be broadly characterized into plume lightning and vent/near-vent discharges (Thomas et al., 2007; Behnke et al., 2013; Cimarelli et al., 2016; Aizawa et al., 2016; Van Eaton et al., 2020). The first modality comprises large-scale discharges at elevation in maturing plumes and, in many regards, is analogous to meteorological lightning (Prata et al., 2020; Van Eaton et al., 2020). Because of the large energies involved, plume lightning can often be detected with wide-range lightning networks (Van Eaton et al. (2020); Prata et al. (2020)). The second category, vent and near-vent discharges, are electrical events that neutralize lower amounts of charge per event and, as their names suggest, occur closer to the volcanic vent (Thomas et al., 2007; Behnke et al., 2013, 2018). Although often lumped together, Behnke et al. (2018) showed that vent and near-vent discharges originate from fundamentally distinct breakdown processes. Vent discharges are innumerable streamer discharges that occur within or directly above the vent and are no more than a few tens of meters in length (Thomas et al., 2007; Behnke et al., 2013, 2018). With current measurement techniques, these minute discharges cannot be detected individually (either at optical or RF wavelengths) or at very great distances. Collectively, however, vent discharges produce a continuous electromagnetic “hum” (commonly referred to as continual radio frequency or CRF) that can be observed with instruments like the lightning mapping array (Thomas et al., 2007; Behnke et al., 2013; Behnke & Bruning, 2015; Behnke et al., 2018). CRF is often detected together with seismic and acoustic signals implying a relationship with explosions and overpressure conditions at the vent (Note: we will use vent-discharges and CRF sources interchangeably) (Smith et al., 2020). Occurring somewhat higher in the column and later in the eruption, near-vent lightning involves leader discharges that can have lengths between a few hundred meters to several kilometers and can be detected individually (Aizawa et al., 2016; Cimarelli et al., 2016; Behnke et al., 2018). Although larger than vent discharges,

near-vent lightning still moves smaller amounts of charge per event than meteorological lightning and, thus, may be invisible to global detection networks (Vossen et al., 2021). Locally, however, it may produce changes to the ambient electric field (Behnke et al., 2018). Aizawa et al. (2016) notes that meteorological/plume lightning shares many characteristics with near-vent lightning, hinting that separating both into two categories may be unnecessary. Nonetheless, an explicit distinction between the two (which we make in the present work) may be warranted given the likely differences in electrification mechanisms underlying near-vent and plume/meteorological lightning.

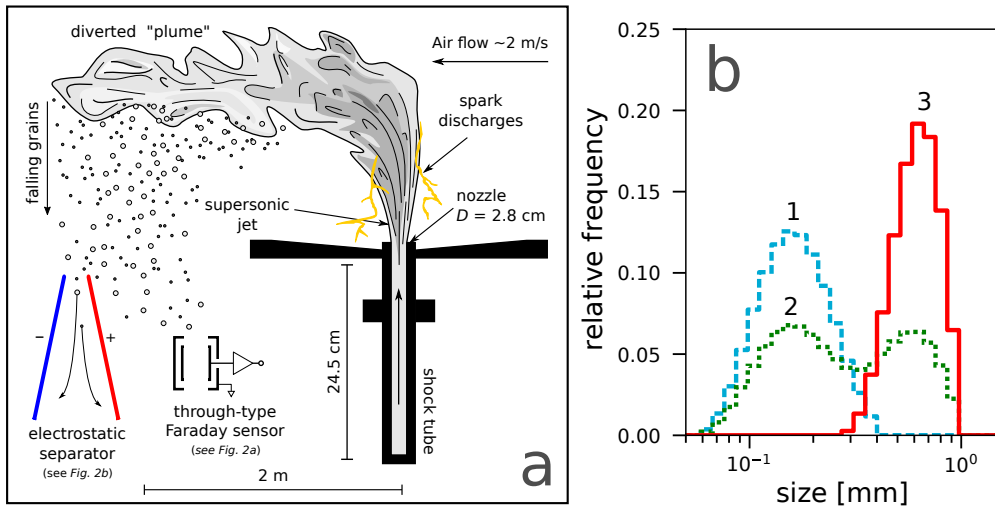


Figure 1: Experimental setup. a) We generate granular jets with the shock-tube setup described previously in Cimarelli et al. (2014). The jet’s dynamics approximate those in the gas-thrust region of volcanic columns and produce spark discharges. Venting into free air, the “column” is then diverted away from the shock-tube by an air stream. Particles falling out of the “plume” are then characterized by two electrostatic measurement systems: 1) an electrostatic separator and 2) a through-type Faraday sensor (described in **Figure 2a** and **b**, respectively). b) Size distributions for the three samples used in these experiments as measured by a diffraction analyzer with the following nominal ranges: 1) 90-300 μm , 2) 50% 90-300 and 50% 300-1000 mixture μm (by volume), and 3) 300-1000 μm .

An ever growing number of observations suggests that vent and near-vent discharges –what we will collectively call proximal discharges– are common during explosive eruptions (Thomas et al., 2007; Behnke et al., 2013; Aizawa et al., 2016; Cimarelli et al., 2016; Behnke et al., 2018; Smith et al., 2020; Vossen et al., 2021). These observations imply that erupted material charges

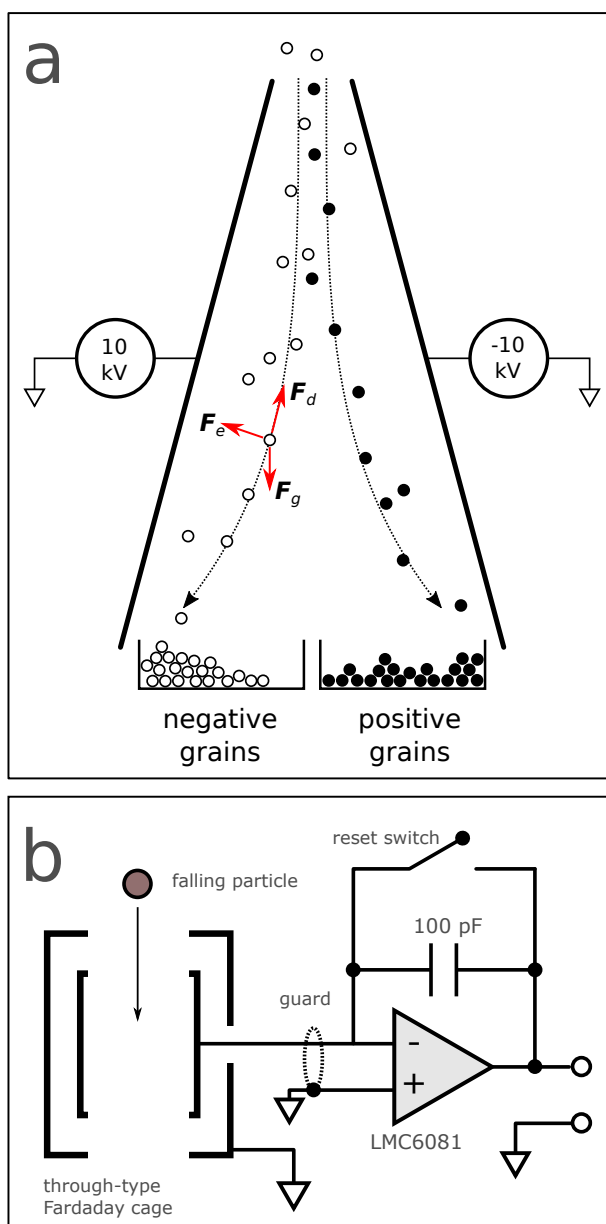


Figure 2: Detail of charge characterization subsystems referred to in **Figure 1**. a) Electrostatic separator to assess the charge polarity on particles as a function of size. Settling grains fall between two plates with a potential difference of 20 kV between them. The electric field separates negative and positive particles and these are collected in two bins at the bottom of the separator. Grains in the bins are then sized using an optical microscope and ImageJ. In this manner, we can investigate how negative and positive charge is partitioned on particles based on size. b) Charge magnitude measurement subsystem. The charge on particles falling out of the “plume” are measured by an array of 8 miniature through-type Faraday cups (TTFC). Each sensor is capable of resolving charges as small as <10 femto-Coulombs (fC). See (Méndez Harper & Dufek, 2016; Méndez Harper et al., 2018b) for more details.

efficiently within the conduit and in the jet-thrust region. Furthermore, there is evidence that proximal discharges contain valuable information about the source of the eruption. For instance, CRF is only detected with forcing at the vent and occurs within the gas-thrust region (Behnke et al., 2018; Smith et al., 2020). Smith et al. (2020) demonstrated this fact by showing that CRF can be correlated with the acoustic and seismic signals associated with active fragmentation. Experimentally, Méndez Harper et al. (2018a) showed that the location and timing CRF emissions reflect the geometry and temporal evolution of barrel shock structures in supersonic jets. These spatiotemporal constraints suggest CRF is a valuable tool to detect incipient eruptions (Behnke et al., 2018). Regarding near-vent lightning, Cimarelli et al. (2016) indicate that the number of discharges is proportional to the over-pressure at the vent. These authors conclude that the intensity of near-vent electrical activity scales with the energy of eruptions. Furthermore, Aizawa et al. (2016) argue that the volumetric charge density in proximal jets may be much larger than that in thunderstorms. Because of these elevated charged loadings, the proximal regions of the volcanic system may also be interrogated using active methods such as GNSS occultation (Méndez Harper et al., 2019). Using an array of electrostatic instruments, Behnke et al. (2018) report complex feedback mechanisms between CRF sources and larger near-vent discharges, suggesting that both forms of discharge may depend on a shared charge budget.

Nonetheless, the physical, chemical, and dynamical processes that charge pyroclasts within the conduit and the gas-thrust region remain poorly constrained. Ice and graupel are generally absent in any large quantities (Cimarelli et al., 2016; Vossen et al., 2021). Thus, in contrast to volcanic lightning at altitude (Van Eaton et al., 2020; Prata et al., 2020), electrification mechanisms comparable to those in thunderclouds cannot account for electrical activity near the vent. Instead, proximal discharges likely reflect “dry” charging processes operating with varying degrees of efficiency within the conduit and an expanding jet.

Starting at depth, material possibly charges during the brittle failure of the magmatic column and subsequent disruptive clast-clast collisions (James et al., 2000). Fractocharging may involve a number of pathways, including piezoelectricity, pyroelectricity, atomic dislocations, positive-hole activation, and the release and capture of positive and negative ions as new surfaces are created (Dickinson et al., 1981; Xie & Li, 2018). James et al. (2000) fractured pumice through repeated impacts and abrasion and found that fragments

carried elevated surface charge densities. Quite recently, Smith et al. (2018) found that eruptions producing more equant grains were associated with CRF, perhaps suggesting that milling (secondary fragmentation) plays a role in vent-discharges. It is worth noting that, although the fracture mechanism is often invoked to account for electrification in the near-vent region, not a single experimental follow up work has been conducted on the matter using natural materials (pumice) in the last 20 years. As such, fractocharging is perhaps the least-well understood “major” charging mechanism in the volcanic context.

Non-disruptive collisions may too lead to electrification through the well-known (but imperfectly understood) triboelectric effect (Hatakeyama & Uchikawa, 1951; Kikuchi & Endoh, 1982; Aplin et al., 2014; Méndez Harper & Dufek, 2016; Méndez Harper et al., 2017, 2020, 2021). Importantly, not only does triboelectricity have the ability to produce efficient charging in a granular material, but may separate charges of opposite polarity based on particle size (Hatakeyama & Uchikawa, 1951; Kikuchi & Endoh, 1982; Zhao et al., 2003; Forward et al., 2009; Waitukaitis et al., 2014). Indeed, triboelectric charging often results in smaller, negatively-charged grains and larger grains with generally positive charges. This phenomenological feature, *size-dependent bipolar charging* (SDBC), may be critical in the production of discharges in proximal volcanic jets (and other dusty planetary environments) as particles of different sizes and opposite charge become separated through hydrodynamics (Cimarelli et al., 2014) or sedimentation (Harrison et al., 2016).

A handful of studies have been explicitly designed to investigate triboelectric SDBC using volcanic materials. Forward et al. (2009) employed a fluidized bed to electrify basalt particles under partial vacuum. This study, however, used heavily altered materials to approximate Martian regoliths rather than recently erupted ash. Nonetheless, serendipitous reports of size-dependent bipolar charging in chemically-unmodified volcanic ash exist in the literature. Many of these observations were not placed within the modern framework of triboelectrification simply because the models had not yet been formulated. Hatakeyama & Uchikawa (1951) studied the frictional electrification of Aso and Asama ash samples. Those investigators reported standard SDBC –that is positive large grains, negative small grains– in Aso ash. However, the Asama ash samples displayed inverse SDBC (negative large grains, positive small grains). In these experiments, particles were allowed to contact foreign objects (an aluminum plate, for example), possibly biasing the polarity of the charge in manners that would not be encountered

in natural systems. Thirty years later, Kikuchi & Endoh (1982) conducted similar experiments and found standard SDBC in ash particles from the 1977 Usu eruption. At Sakurajima, Miura et al. (2002) measured changes in the atmospheric potential gradient associated with small explosive events and estimated the surface charge density and polarity of ash falling out of plumes using an electrostatic separator (a method similar to the one we describe below). Those authors report particles with surface charge densities approaching the ionization limit (10^{-6} - 10^{-5} Cm⁻²) and standard SDBC.

In addition to tribo- and fractoelectric processes, other mechanisms have been proposed to account for proximal discharges. Pahtz et al. (2010) suggests that materials like volcanic ash and mineral dust could charge through the polarizing effects of an ambient electric field. Aplin et al. (2014) provide evidence that the decay of radioactive elements in the magma may lead to “self-charging” of ash. Very recently, Nicoll et al. (2019) deployed sensors into a plume at Stromboli, finding that the gas phase itself is charged.

Building monitoring tools that effectively leverage proximal electrical effects requires a better understanding of the mechanisms that charge pyroclasts. Accomplishing such a feat, however, is complicated by the fact that much uncertainty remains regarding proposed electrification mechanisms themselves. For instance, while triboelectrification has been described since the time of the ancient Greeks, we have yet to unequivocally identify the charge carriers being exchanged during frictional interactions (Lacks & Sankaran, 2011; Lacks & Shinbrot, 2019). These charge carriers could be electrons, ions, or both. Similarly, some authors have presented evidence that triboelectrification arises from surface damage at minute spatial scales, implying that contact and frictional electrification are ultimately forms of fragmentation charging (Pan & Zhang, 2019; Lacks & Shinbrot, 2019).

Beyond questions surrounding the charging mechanisms that putatively drive vent and near-vent discharges, little is known about how proximal electrification influences the long term electrostatic evolution of the eruptive column. One possibility is that pyroclasts advected high into the atmosphere retain charge generated in the conduit and the gas-thrust region. This “pre-charging” may have important consequences for subsequent electrical effects, as some work indicates that charging in a granular material depends on pre-existing electric fields (e.g. Pahtz et al. (2010)). A second possibility is that the abundance of proximal discharges effectively neutralizes charge gained at or near the vent. Recombination in the gas-thrust region would imply that “downstream” lightning storms in mature plumes generally necessitate addi-

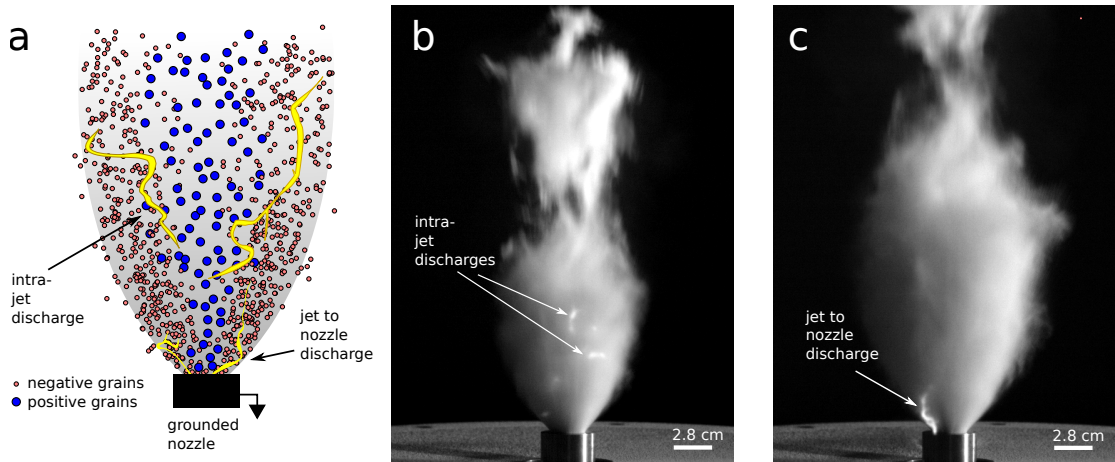


Figure 3: a) Schematic showing two kinds of discharge in the experiments. 1) Intra-jet discharges occur between grains or clusters of grains of opposite polarity. 2) Jet to nozzle discharges occur between the charged grains and grounded metallic nozzle. b) Typical intra-jet discharges in an experiment with the 90-300 μm particle size distribution. c) Jet to nozzle discharge in the same experiment as b).

tional cycles of electrification (perhaps driven by ice) and reflect little about eruption dynamics at the source. Evidence for this second hypothesis exists in field data collected at Augustine (Thomas et al., 2007) and Redoubt (Behnke et al., 2013), which show that electrical activity waned after the initial explosive phases. These periods of electrical inactivity could signify that volcanic columns emerge from the gas-thrust region with weak degrees of charging. The resumption of electrical activity in mature plumes could indicate activation of water-based electrification mechanisms (Prata et al., 2020; Van Eaton et al., 2020).

Here, we use a shock-tube to simulate explosive, overpressured volcanic jets and address a subset of the questions posed above. Our setup allows us to investigate the charge mechanisms that drive CRF sources and make inferences regarding subsequent near-vent lightning. For the first time, we identify nominal size-dependent bipolar charging in a simulated volcanic jet bearing streamer discharges. SDBC in our shock-tube experiments provides direct evidence that tribocharging is a dominant electrification mechanism in the gas-thrust region. Additionally, we find that particles emerging from the supersonic flow carry charge densities comparable to those measured on

grains falling out of proximal volcanic columns (e.g. Gilbert et al. (1991); Miura et al. (2002)). Further analysis shows that this amount of charge may be sufficient to drive near-vent lightning. As such, our results indicate that near-vent lightning is likely underpinned by the same electrification mechanisms as CRF sources, but reflects larger scale charge separation in columns.

2. Methodology

We use the shock-tube setup described previously by Cimorelli et al. (2014) to produce artificial volcanic discharges (**Figure 1a**). The shock-tube (24.5 cm in length, 2.8 cm in diameter) was loaded with approximately 75 ml of volcanic ash and then pressurized to 10 MPa with argon gas. Exceeding this pressure ruptures a set of two diaphragms, causing the granular material to be ejected from the tube by explosive decompression. The dynamics of the decompression event and the resulting supersonic jet simulate those expected in the conduit and gas-thrust region of a volcanic jet (Cimorelli et al., 2014; Gaudin & Cimorelli, 2019). This apparatus has the ability to charge pyroclasts through two principal mechanisms: fractoelectrification and tribocharging. The contributions from other putative electrification mechanisms such as radioactive decay or induction are excluded.

Unlike previous efforts in which the shock-tube vented into a metallic collection chamber, we allowed the jet to expand into a large room to minimize collisions between grains and foreign surfaces. A low-powered air stream with a velocity of 2 m/s was generated perpendicular to the flow at a height of 1 m above the nozzle (~ 80 cm above the Mach disk). This artificial “wind” was used to deflect lofted particles away from the ejection axis (see schematic in **Figure 1a**). Pushed away from the shock-tube and falling under the action of gravity, grains were sampled by two devices: 1) an electrostatic separator (ESS) and 2) an array of eight miniature through-type Faraday cages (TTFC) capable of measuring the charge on individual grains. Both the ESS and TTFC array were placed 1.5 m downwind of the nozzle. We note that a principal source of error associated with this methodology is that the size distribution of sampled particles may be different from that of the original sample. As discussed in Cimorelli et al. (2014), experimental flows composed of larger particles are dominated by inertia. Thus, these particles were difficult to deflect using the artificial wind. Additionally, if successfully deflected, larger particles may fall out of the plume before they reach

the sensors. We attempted to compensate for these effects by strategically placing the sensors in the proximity of the shock-tube, but we note that the constraints of the laboratory environment could not completely alleviate them. The overall result is that our measurement technique is better suited to characterize samples with fine grain size distributions.

The ESS consists of two vertical, sub-parallel, 1 m-long copper plates with a potential difference of 20 kV between them (See **Figure 2a**). When a charged particle passes between these plates, its trajectory is modified by the imposed electric field. Negatively-charged grains are diverted toward the positive plate, whereas grains carrying positive charge drift toward the negative plate. Thus, particles were separated by polarity and collected in two bins placed at the base of the separator. We then characterized the particles with an optical microscope to obtain spherical-equivalent diameters.

The TTFC array was micromachined directly onto a printed circuit board. Each Faraday cup has an aperture of 1 mm and is capable of measuring charges <10 fC. A simplified schematic for a single channel of the TTFC is shown in **Figure 2b**. When a particle traverses the sensing volume of one of the TTFC channels, an amplifying stage produces a voltage pulse whose magnitude is proportional to the charge on the particles. This output voltage was digitized by a National Instruments NI-6008 data acquisition unit and a PC running LabVIEW.

Each shock-tube decompression event was recorded with a high-speed camera at a frame rate of 36,000 fps, allowing us to capture discrete spark discharges in the flow. We employed washed and sieved pumice quarried from deposits of the 13 ka Laacher See maar eruption in the Eifel Volcanic Field (Germany) with three different granulometries: fine (nominally 90-300 μm), coarse (nominally 300-1000 μm), and medium (a 50/50 mixture by volume of the fine and coarse samples). Particle size distributions before the experiments were obtained with a Coulter LS230 laser sizer. Because the number of particles sampled per experiment by both the ESS and the TTFC is relatively low, we repeated each experiment four times with each granulometry.

3. Results and discussion

3.0.1. Electrical discharges

All experimental jets produced electrical discharges. A typical electrical spark in an experiment using the 90-300 μm sample is rendered in **Figure 3**.

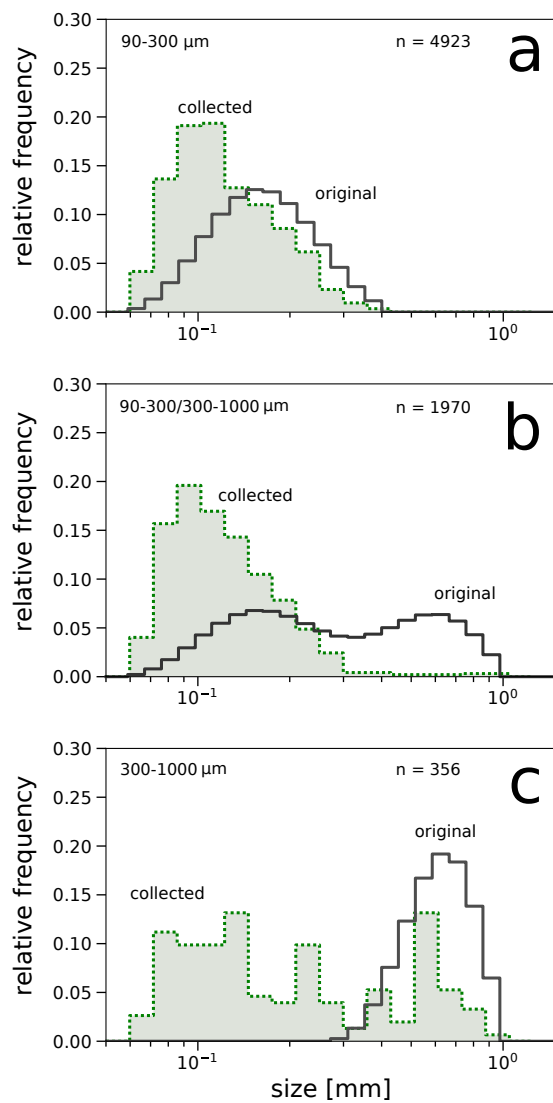


Figure 4: Particle size distributions for particles collected in the electrostatic separator (dotted green, filled) and original sample (solid black, unfilled); a) 90-300 μm ; b) 90-300 and 300-1000 μm (at 1:1 weight ratio); and c) 300-1000 μm . The number of particles characterized per collected sample is indicated in the top right of each panel.

We observed discharges exclusively within the region of rarefying jet expansion as described by Méndez Harper et al. (2018a) (we note that discharges could have also occurred within the shock-tube itself, but we were unable to image these). As reported by Cimorelli et al. (2014) and Gaudin & Cimorelli (2019), we find that the number of discharges generally increased with the proportion of fines. Experiments with the fine granulometry displayed innumerable small discharges, whereas jets with coarse particles produced no more than a dozen discharges events per experiment. Cimorelli et al. (2014) suggest that these distinct behaviors underscore differences in gas-particle coupling between experiments. Specifically, in jets with abundant fines particles cluster in turbulent eddies. Conversely, in experiments with coarse grains, the motion of particles remains collimated by inertia. These dynamics depend on SDBC.

We clarify that the discharges we observe in our experiments are not representative of large scale lightning, volcanic or otherwise. The small sparks described here and in previous works (e.g. Gaudin & Cimorelli (2019); Stern et al. (2019)) are cold plasma channels or corona streamers, rather than highly conductive, hot leaders. Many of us have experienced the (startling) effects of streamers when reaching for a doorknob after scuffing our shoes on a carpeted floor. As noted above, Behnke et al. (2018) hypothesize that CRF may be the collective manifestation of many streamers occurring at the vent of an erupting volcano. We consider the discharges in our experiments to be laboratory analogs of these CRF-generating streamers.

3.1. Grain size distributions

Particles in the jet were diverted by a horizontal air stream toward an electrostatic separator and a Faraday cup array. We sized the grains that fell into the ESS using an optical microscope. The size distributions for each sample are rendered in **Figure 4** (green, filled curves). These histograms aggregate data from four shock-tube experiments. For reference, the pre-experiment size distributions as measured by a diffraction-based size analyzer are also displayed in **Figure 4** (unfilled, solid curves).

By comparing the pre- and post-experiment histograms in **Figure 4**, we see that the experimental process modified the original size distributions in two principal ways. Firstly, as discussed above, smaller particles were diverted in greater number than larger ones by the stream of air. Thus, the material collected in the ESS was biased toward the smaller grains. Such effect was more noticeable for samples containing particles in the 300-1000

μm size range (**Figure 4c** and **b**). Furthermore, the total number of particles collected by the separator decreased as the abundance of large particles increased (we report the total number of particles sampled in the upper right corners of panels in **Figure 4c**). A second effect, evident in **Figure 4**, was the presence of particles smaller than the smallest grain in the original sample. This implies that some amount of material was disrupted during the decompression event and/or subsequent transport (Dufek et al., 2012). These two effects are worth considering as we discuss the possible electrification mechanisms present in our experiments.

3.2. Size-dependent bipolar charging

Grains leaving the spark-bearing jet fell through the ESS (**Figure 1b**), where they passed through a strong electric field and were separated by charge polarity. The size distributions for the negative and positive samples for each granulometry as measured using an optical microscope are shown in **Figure 5** (negative: unfilled, blue curves; positive: filled, red dotted curves). Again, each histogram aggregates data from four separate experiments. The sums of these histograms result in the total post-experiment histograms in **Figure 4**. For both the small and medium distributions, we observe clear size-dependent bipolar charging. Negatively charged particles (blue, unfilled histograms in **Figure 5**) were more likely to have smaller diameters than positively charged grains (red, filled histograms). We did not detect statistically significant SDBC in the large sample. We suspect that this absence stems from the sampling limitations discussed above rather than the charging characteristics of the granular sample itself.

This partitioning of charge polarity among particles of different sizes in the small and medium samples is consistent with previous descriptions of triboelectricity in granular materials (Zhao et al., 2003; Forward et al., 2009; Waitukaitis et al., 2014; Toth III et al., 2017). As noted by Forward et al. (2009), such size effect appears to be a universal characteristic of chemically-homogeneous triboelectrification. Yet, despite the large number of works that report SDBC, the microphysical processes that cause particles of different sizes to concentrate charge of opposite polarities remain obscure. Some authors have invoked an exchange of trapped electrons between surfaces to account for SDBC (Lacks & Levandovsky, 2007; Forward et al., 2009). The trapped electron model proposes that all material surfaces have electrons caught in unfavorable high-energy states. Surfaces are also assumed to have an even larger number of empty, low-energy states. For insulating particles,

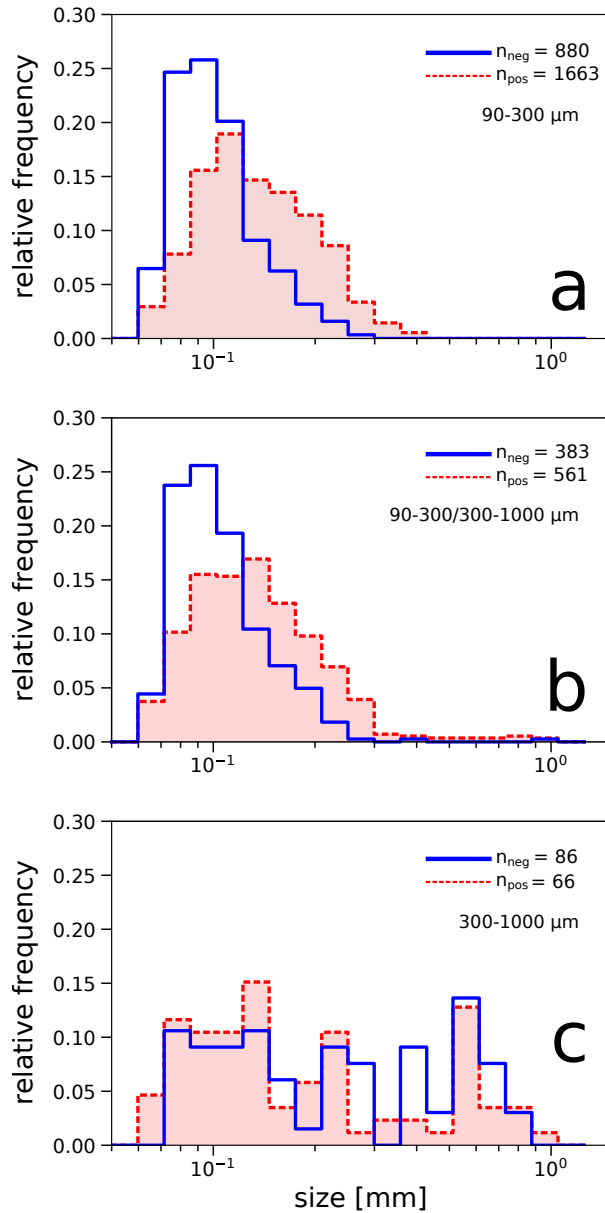


Figure 5: Particle size distributions for positive (red, filled) and negative (blue, empty) particles collected by the electrostatic separator; a) 90-300 μm ; b) 90-300 and 300-1000 μm (at 1:1 weight ratio); and c) 300-1000 μm . Number of positive (n_{pos}) and negative (n_{neg}) particles analyzed are reported in the red and blue text respectively. Charge partitioning among particles of different sizes occurs for all granulometries, but is more pronounced for the samples containing small particles (90-300 μm).

high- and low-energy states on the same particle surface cannot readily recombine because of the material’s low conductivity. When two particles are brought into contact, however, there is a finite probability that a trapped electron on one surface will transfer to a low-energy state on another. Although particles of different sizes have the same density of trapped electrons, the net number of trapped electrons should scale with particle size. Thus, after a comparatively low number of contacts, smaller particles may become depleted in high-energy, donor electrons. Yet, small particles may continue to fill vacant, low-energy states with electrons transferred from large particles. Over time, there is a net transfer of negative charge from electron-rich, large particles to smaller ones (Lacks & Levandovsky, 2007; Forward et al., 2009).

Despite the trapped electron model’s ability to account for the general features of same-material tribocharging, Waitukaitis et al. (2014) have argued that the density of trapped, donor electrons on surfaces may be insufficient to produce the degrees of charging observed in granular media. Recent work posits that, rather than electrons, the main charge carriers exchanged during particle-particle collisions are water ions (Gu et al., 2013). This water ion partitioning model brings attention to water films that naturally exist on most surfaces in atmosphere. Within these films, water molecules undergo self-ionization to produce OH^- and H^+ . During grain-grain collisions, some mechanical energy is converted to heat. The temperature of smaller particles climbs faster than that of larger grains. Because H^+ has a higher mobility than the heavier OH^- , positive charge is able to efficiently migrate from a warm, small grain to a large, cool grain. Thus, the water ion partitioning model leads to the same qualitative conclusion as the trapped electron model: small, negative particles and large, positive particles. Ultimately, the mechanisms that bring about SDBC in granular media are an area of active research and it is difficult to point to a single mechanism with any certainty at this time.

While SDBC may be a diagnostic property of triboelectrification, we consider whether such phenomenon occurs in other electrification mechanisms as well. Such attention is warranted because the ESS collected particles smaller than the smallest grains in the original sample (this effect is particularly evident in the experiments with the large granulometry; see **Figure 5c**). The presence of these fine particles –presumably produced by the disruption of larger particles during the decompression events– suggests that some amount of fragmentation charging was active during each experiment.

In the context of fractocharging, charge partitioning based on size has been reported at least once. By breaking a variety of pumice samples, James et al. (2000) found that larger and smaller fragments gained opposite charge polarities. This *fracto-SDBC*, however, varied significantly from that generally observed in frictional electrification. Foremost, James et al. (2000) found that (in general) larger fragments carried negative charge, whereas small particles charged positively—opposite to that associated with triboelectricity. Additionally, the authors deduced that fracto-SDBC reflects longer, secondary processes—namely, the asymmetric capture of positive ions by particles settling at different velocities—rather than charge rearrangements occurring during the fracture process itself. James et al. (2000) themselves noted that charge polarity segregation is not likely to occur during fragmentation because “any section of fracture surface has no knowledge of the size of particle to which it is attached.” Thus, while fractocharging may efficiently produce elevated charge densities on newly-formed surfaces, the polarity of any given fragment immediately after fracture may involve greater stochasticity. Such behavior stands in contrast to tribo-SDBC, where charge partitioning is believed to occur at the moment two surfaces touch and separate. The expedient nature of SDBC has been demonstrated explicitly in free-fall experiments using high-speed videography (Waitukaitis et al., 2014). Those investigations reveal charge and charge separation processes occurring on millisecond timescales and imply faster rates for granular media with higher granular temperatures. Conversely, charge partitioning in the fracture mechanism seems to depend on how fast fragments can scavenge ions. James et al. (2000) report minute-long timescales for this process. Ultimately, whether or not SDBC is an inherent property of fractoelectric charging (or any other mechanism), as it appears to be in triboelectric ones, remains an open question and should be the focus of future dedicated studies.

3.3. Charge density on fallout

The ESS allowed us to determine the distribution of charge polarity on grains falling out of the diverted jet, but not charge magnitude. We used an array of 8 through-type Faraday cups to assess the charge magnitude on particles (**Figures 1a** and **2b**). Particles traversing the sensing volume of a cup produced voltage pulses at the output of an amplification circuit (exemplified in **Figure 6a**). The amplitudes of the pulses were proportional to the charge on the sampled particles. The histograms in **Figure 6b** show the distributions of charge on particles in four experiments for each of the

three samples. **Figure 6c** displays the absolute magnitude of that same data on a logarithmic scale. The hard cut-off near $3 \times 10^{-14} \text{ Cm}^{-2}$ represents the noise floor of the TTFC. In agreement with the ESS measurements, we find that particles traversing the TTFC array carried both negative and positive charge with a mean charge near zero Coulombs.

A common way to characterize charging in a granular material is to compute particle surface charge density –that is, the charge normalized by the particle surface area. Because our array of TTFC did not allow for simultaneous measurements of charge and size, we present the surface charge density σ as the joint probability given a grain size distribution (using spherical equivalent diameters) and the distribution of measured absolute charges (**Figure 6c**). The cumulative probability distributions of surface charge density for the three granulometries are shown in **Figure 7**. We compute charge densities using both the pre- and post-experiment grain size distributions (**Figure 4**). In **Figure 7**, the dashed purple curves represent the charge densities computed with the post-experiment granulometry, whereas the solid purple curves are the charge densities computed with the pre-experiment grain size distributions. The grey area between the curves represents the uncertainty involved in these computations. For comparison, **Figure 7c** displays the maximum charge densities measured on ice, graupel (i/g), and rain within East Asian rain bands (Takahashi, 2012), as well as ash falling out of a Sakurajima plumes (Gilbert et al., 1991; Miura et al., 2002). We discuss these comparisons further on.

By invoking Gauss’ Law, the theoretical maximum surface charge density on a large surface can be computed as:

$$\sigma_{\max} = \epsilon_r \epsilon_o E_{\max}. \quad (1)$$

Above, $\epsilon_o = 8.854 \times 10^{-12} \text{ F m}^{-1}$ is the permittivity of vacuum, ϵ_r is the relative permittivity of gas phase, and E_{\max} is the breakdown electric field of the gas for a given pressure. We set the relative permittivity equal to 1 and $E_{\max} = 3 \times 10^6 \text{ Vm}^{-1}$ (corresponding to conditions within the lab). The theoretical maximum charge density σ_{\max} is then $2.66 \times 10^{-5} \text{ Cm}^{-2}$. This threshold is indicated in **Figure 7** by the vertical, red lines (panel a and b) and a triangle (panel c).

Our data shows that the surface charge density on grains spans several orders of magnitude up to the theoretical breakdown limit. However, we find that for all experiments the probability that a particle will have a charge

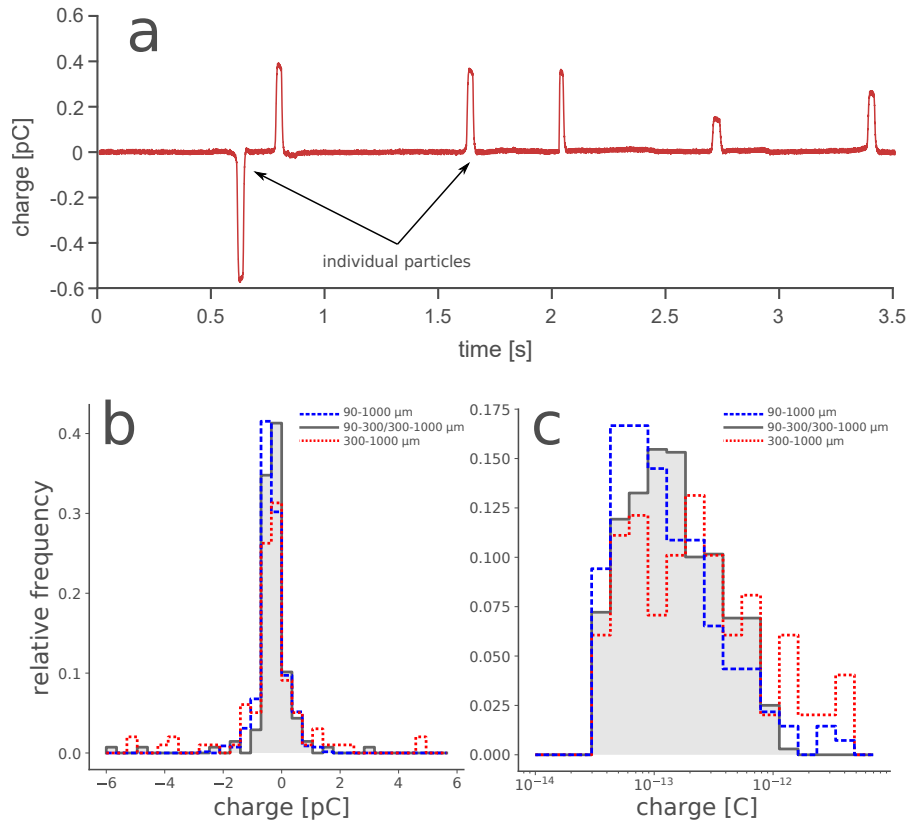


Figure 6: a) Output from one TTFC amplifying stage. Each pulse is representative of the charge on an individual grain traversing the sensing volume. b) The distribution of surface charge on individual particles for each granulometry (dashed blue: 90-300 μm ; solid grey: 90-300/300-1000 μm ; dotted red: 300-1000 μm). The distributions represent the aggregation of data collected across four experiments. Particles charge both positively and negatively and had mean charges near 0 Coulombs. c) Same as b) but plotted on a logarithmic scale (absolute charge).

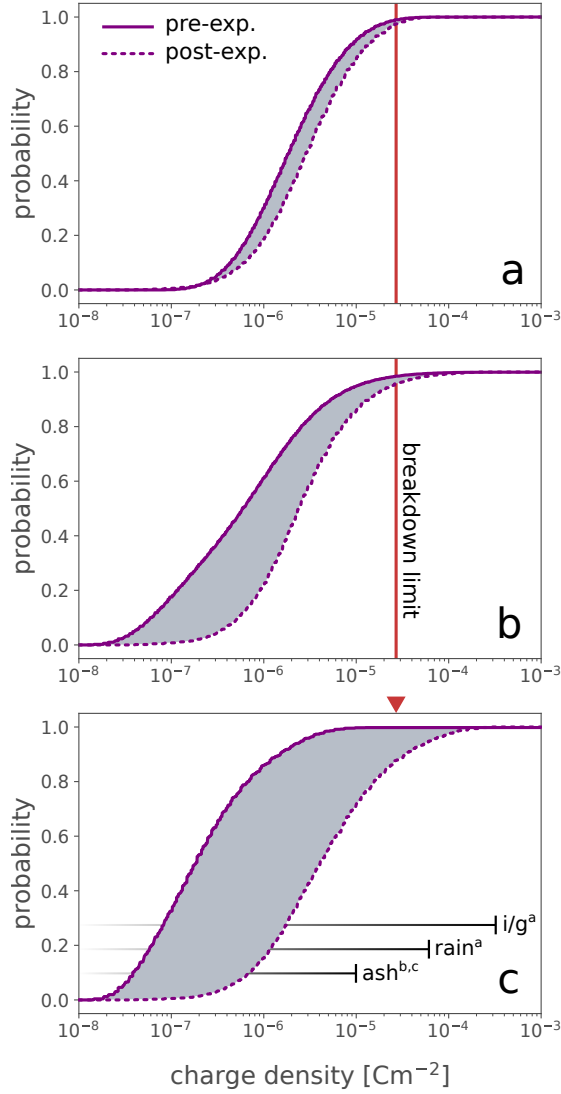


Figure 7: Cumulative probability distributions of surface charge density for the three samples as inferred from the size distributions in **Figure 4** and charge distributions in **Figure 6**. Note that this surface charge density calculation was done for both the pre- and post-experiment size distributions. a) 90-300 μm ; b) 90-300 and 300-1000 μm (at 1:1 weight ratio); and c) 300-1000 μm . The vertical red lines in panels a) and b) and the triangle in panel c) indicate the theoretical maximum surface charge density for large surfaces (**Equation 1**). The horizontal bars in panel c) indicate the ranges of surface charge densities measured on particles in the field: ice and graupel (abbreviated i/g) (Takahashi, 2012), rain (Takahashi, 2012), and volcanic ash (Gilbert et al., 1991; Miura et al., 2002).

density exceeding this threshold ranges between 2% and 13% depending on the grain size distribution (pre- or post-experiment) used to compute the surface charge density distributions. In other words, particles falling out of the diverted plume are overwhelmingly under-saturated in charge according to **Equation 1**. This apparent under-saturation may result from the fact that we characterized the charge on grains after they transited the region of the jet where discharges occur. As such, we may be measuring only a fraction of the initial charge generated during the decompression event. Indeed, as described in Méndez Harper et al. (2018a), the compressible gas dynamics within the barrel shock may lead to a region of weakened dielectric strength in which particles are forced to shed charge. However, as noted in Gilbert et al. (1991), particles in dry granular media are rarely observed to carry surface charge densities exceeding 10^{-5} Cm^{-2} . Apparent low surface charge densities on individual grains may simply result from how charge carriers arrange themselves on dielectric surfaces. Baytekin et al. (2011) demonstrated that charge may not be distributed uniformly on insulating surfaces. Owing to their high surface resistivities, charged dielectrics can display coexisting regions of high and low surface charge density. Furthermore, these areas need not be of the same polarity. Because a TTFC measures the *net* charge on a particle passing through its sensing volume, the sensor cannot resolve distinct regions of negative and positive charge on grains even if those individual areas have charge densities close to the breakdown limit.

Interestingly (and for comparison), measurements of charge on hydrometeors in thunderclouds reveal that ice, graupel, and rain may carry net charge densities substantially higher than those carried by silicate grains (**Figure 7c**). Takahashi (2012), for instance, revealed that $500 \mu\text{m}$ ice and graupel particles in East Asian rainbands had charges as high as 100 pC, implying surface charge densities in excess of 10^{-4} Cm^{-2} . These elevated particle charge densities indicate that ice-based charging mechanisms in thunderstorms may be more efficient than dusty triboelectrification.

4. Implications for electrical processes in volcanic jets

4.1. Charging mechanisms in the near vent region

Although size-dependent bipolar charging has been described before in mobilized volcanic ash (Hatakeyama & Uchikawa, 1951; Kikuchi & Endoh, 1982; Miura et al., 2002), our experiments are the first (as far as we are aware) to detect this charge partitioning in spark discharge-bearing granular flows.

The presence of SDBC in our shock-tube experiments, designed to replicate the dynamical conditions in the conduit and gas-thrust region, provides direct evidence that tribocharging is a primary electrification mechanism in near-vent volcanic jets and may be responsible for proximal discharges. Although, Behnke et al. (2018) found that changes to ambient electric fields are absent during continual RF emissions (indicating that overall negative and positive regions in a jet have not yet formed), Cimarelli et al. (2014) suggest that centimeter to meter long filamentary discharges would still require some amount of charge separation on small spatial scales. Such charge separation may be driven by turbulent eddies in the flow. Furthermore, this clustering needs to occur on relatively short timescales (a few milliseconds in the case of our shock-tube). Size-dependent triboelectrification meets these criteria given that collisions simultaneously generate charge and distribute charges of opposite polarities among grains of different size (Waitukaitis et al., 2014). Simulations of triboelectricity in granular materials (e.g. Duff & Lacks (2008)) imply that the speed at which these co-joined processes occur scales with collision frequency. Because of the high particle loading and turbulent kinematics in the gas-thrust region, we suspect that tribocharging and charge separation rates may be very efficient in incipient jets.

Other proposed “ice-free” mechanisms may also generate high levels of charge on short timescales within the gas-thrust region. The fragmentation of the magma column or disruptive clast-clast collisions, for example, likely electrify fragments across periods of micro- or even nanoseconds (the duration of active crack propagation). Yet, available experimental data indicates that the segregation of negative from positive fragments happens independently of the fragmentation process and may require substantially longer periods to manifest (James et al., 2000). Thus, the rapid clustering of negative and positive particles based on size described above may not occur. However, CRF could also be produced by smaller discharges than the proposed 1-10 m sparks in volcanic columns or even the cm-scale discharges in our shock-tube jets. Indeed, Méndez Harper et al. (2021) have electronically observed spark discharges in granular basalt flows with poor sorting. Unlike the spark discharges in our shock-tube which can be observed directly with an antenna connected to an oscilloscope, the discharges reported in Méndez Harper et al. (2021) require an amplification stage to be detected. Wurm et al. (2019), working in the context of discharges in Martian dust storms, hypothesize the existence of micro-scale discharges between individual grains or glow discharge between a grain’s surface and the atmosphere. These grain-grain

discharges would require very little clustering and could be driven directly by the high levels of charging associated with fractoelectrification. Whether or not the collective action of such minute discharges could produce or enhance CRF would be an interesting topic for future research.

Because our shock-tube does not simulate dynamics beyond the gas-thrust region and each experiment lasts a few milliseconds, we cannot directly comment on any longer charge segregation processes. Nonetheless, field data suggests that these may become important as jets evolve into buoyant plumes. Miura et al. (2002) characterized changes in the local electric field during small explosions at Sakurajima. Based on these measurements and assessment of charged fallout, they conclude that Sakurajima plumes consisted of a principal negative charge layer sandwiched between two positive layers. Miura et al. (2002) suggest that this positive-negative-positive arrangement comprises a lower region of coarse, positive particles, a middle section of fine, negatively-charged ash, and a top layer of positive gas or aerosols. The charge separation in the two lowermost layers is consistent with standard SDBC associated with triboelectrification. However, current triboelectric models and our data cannot account for the topmost layer. Such layer may originate from material fracture, as described by James et al. (2000), or the decay of radon gas (Nicoll et al., 2019). The low elevations of Sakurajima plumes (< 4 km), as also observed by more recent studies (Cimarelli et al., 2016; Vossen et al., 2021), make it unlikely that ice-based charging mechanisms were responsible for observations made by Miura et al. (2002). Together, our experimental data, that of James et al. (2000), and field observations suggest that proximal discharges are driven by triboelectrification in conjunction with another mechanism—likely fractoelectrification.

4.2. Electrical effects beyond the gas thrust region

Although our shock-tube experiment does not replicate the physics underlying the generation of near-vent lightning, the measurements of charged particles falling out of a simulated jet allow us to make basic inferences about the electrostatic conditions downstream of the gas-thrust region. Given that near-vent lightning tends to occur immediately after or even concurrently with CRF discharges (Behnke et al., 2018), it may be reasonable to assume that both electrical phenomena are driven by the same electrification mechanisms.

Observations at Sakurajima reveal that near-vent discharges, with lengths ranging between 10-400 m, are essentially scaled-down equivalents of thun-

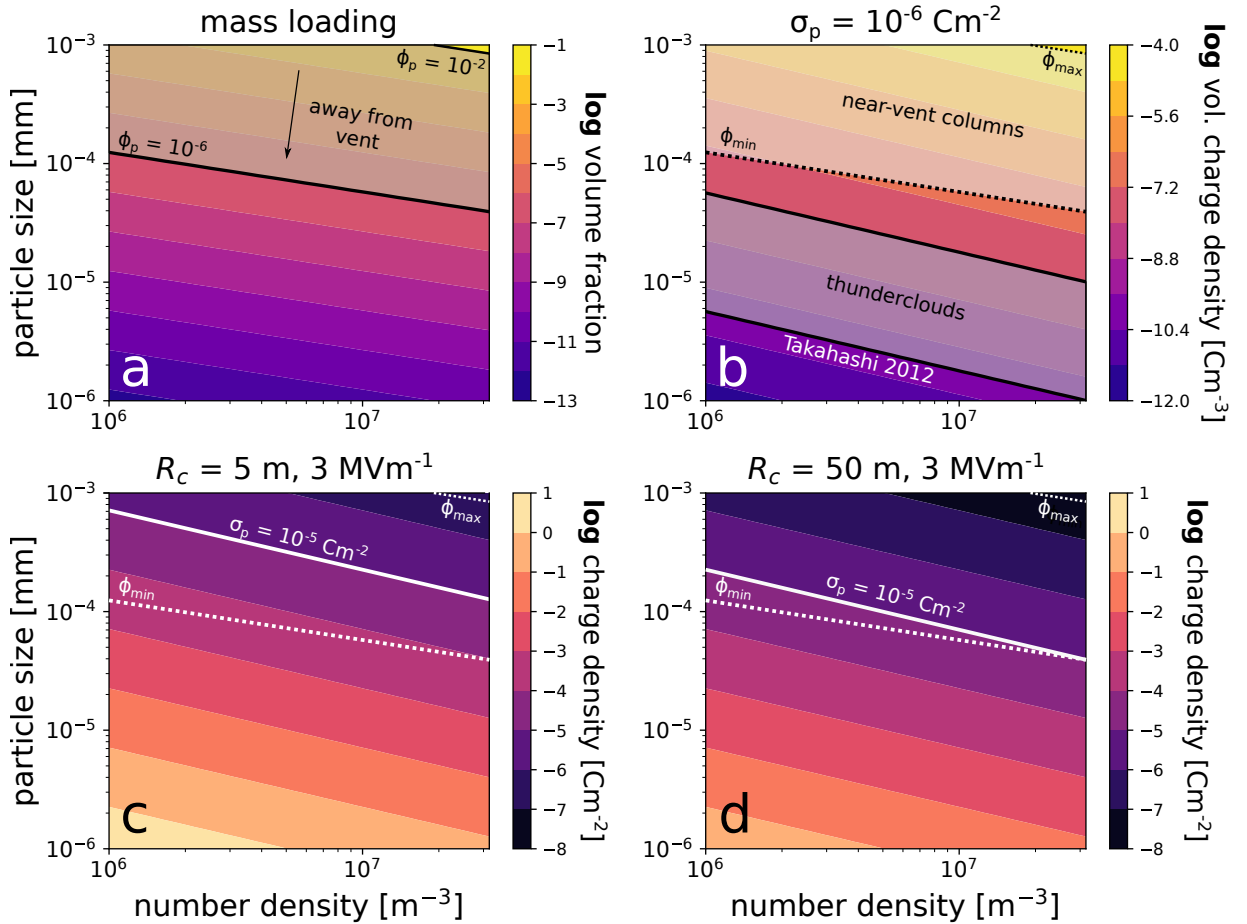


Figure 8: Breakdown criteria for a volcanic ash cloud. a) Mass loading as a function of particle size and particle number density. Shaded region denotes mass loadings expected for proximal columns (see references within text). b) Volumetric charge density as a function of particle size and number density assuming grains with surface charge densities on the order of 10^{-6} Cm^{-2} . Shaded upper region indicates expected volumetric charge densities for proximal columns. Shaded lower area indicates range of volume charge densities measured in thunderclouds (Takahashi, 2012). c) Surface charge densities required to produce an electric field at the edge of the region of 3 MVm^{-1} as function of particle size and number density. Region radius set to 5 m. d) Same as c) but for a radius of 50 m.

derstorm lightning (Aizawa et al., 2016; Cimorelli et al., 2016) (we note that, in general, vent-discharges can be longer than those observed at Sakurajima). Unlike CRF sources, near-vent discharges appear to rely on the presence of meso-scale electric fields, indicating the formation of negative and positive regions in a convectively rising column (Behnke & Bruning, 2015; Behnke et al., 2018). In their report on Sakurajima near-vent lightning, Aizawa et al. (2016) present a simple model to describe the relationship between flash length and volumetric charge density in these regions. Those authors conclude that near-vent lightning requires small regions of high volumetric charge density. Here, we take this analysis further using the data from our experiments. Assuming each of the charged regions is spherical (radius: R_r , radius: A_r , volume: V_r), we can place first-order constraints on the breakdown conditions given the surface charge densities rendered in **Figure 7**. The electric field E_s at the surface of the region must satisfy Gauss’s Law:

$$E_s \oint dA_r = \frac{Q(n, A_p, \sigma_p)}{\epsilon_r \epsilon_o}. \quad (2)$$

Above, Q is the total charge in the region, which depends on the number density of grains n , the total particle surface area A_p , and the particle surface charge density σ_p :

$$Q = \sigma_p A_p V_r n. \quad (3)$$

Let us consider a region where n is in the range of 10^6 - 10^8 m^{-3} and the particle diameter is $D_p = 10^{-3}$ - 10^{-6} m. This results in volume fractions spanning $\phi = 10^{-13}$ - 10^{-1} , the higher portion of which ($\phi_{min} = 10^{-5}$, $\phi_{max} = 10^{-2}$) applies to near-vent volcanic columns (Suzuki et al. (2016); Del Bello et al. (2017); see shaded area in **Figure 8a**). Assuming any given particle in the region has a charge density on the order of 10^{-6} Cm^{-2} (the typical charge density per particle measured on grains falling out of our experimental jets and that measured on from Sakurajima plumes by Miura et al. (2002)), we can compute the region’s volumetric charge density as:

$$\rho = \pi \sigma_p D_p^2 n \quad (4)$$

This calculation is shown in **Figure 8b**, where, for comparison, we have also plotted the volumetric charge densities in conventional thunderclouds as measured by radiosondes (Takahashi (2012) and references therein; shaded

area). Despite its simplicity, this analytical model is consistent with inferences made by Aizawa et al. (2016) regarding the charge content of Sakurajima columns. Specifically, we expect the volumetric charge density to be much larger in nascent columns (ranging between 10^{-4} Cm^{-3} near the vent and 10^{-7} Cm^{-3} toward the edge of the gas thrust region) than in conventional thunderstorms (ranging between 10^{-10} and 10^{-8} Cm^{-3} ; Takahashi (2012)), despite the fact that individual hydrometeors may carry substantially higher surface charge densities than pyroclasts.

We can also estimate the surface charge density per particle required to produce the breakdown field E_s at the surface of the region for given region size, particle size, and volume fraction. Solving **Equation 2** for the particle charge density yields:

$$\sigma_p = \frac{3E_s \epsilon_r \epsilon_o}{\pi D_p^2 n R_r}. \quad (5)$$

For demonstration purposes, let us set the surface breakdown field to the classical ionization limit of $E_s = 3 \text{ MVm}^{-1}$ (this value would be halved if we are considering two adjacent, oppositely charged regions). We perform these calculations for regions with radii of 5 and 50 m (displayed, respectively, in **Figure 8c** and **d**), based on the characteristic length of near-vent lightning events described in Cimarelli et al. (2016) (10s - 100s m). **Figure 8c** and **d** show that for jets with volume fractions in the range of $\phi = 10^{-6}$ - 10^{-2} , the particle charge densities measured in our experiments (10^{-8} - 10^{-5} Cm^{-2}) would be sufficient to produce edge electric fields on the order of MVm^{-1} . We note that maximum electric fields measured in thunderclouds are generally an order of magnitude smaller than the classical limit, suggesting that lightning initiation is controlled by processes other than conventional dielectric breakdown (Petersen et al., 2008). Assuming similar initiation processes in jets, individual pyroclasts may not need to carry very high net charge densities to meet the lightning initiation criteria if the flow is dense enough (i.e. high mass loading). Additionally, abundant particles may serve to locally enhance a background field, as has been modelled by a number of authors in the context of thunderclouds, reducing the need for extensive, high-magnitude electric fields (Dwyer & Uman, 2014).

As a column matures into a plume, the fate of charge gained in gas thrust region becomes less certain. As noted above, observations at Augustine and Redoubt revealed periods of electrical inactivity following decreases in rates of vent discharges and near-vent lightning (Thomas et al., 2007; Behnke

et al., 2013, 2018). One possibility is that as the column entrains air and expands, the volumetric charge density decreases to the point where breakdown conditions are no longer satisfied. Additionally, eruption columns may have been relatively dry during their initial phases. As they cool, however, condensing water, either magmatic or environmental, may promote charge leakage. Although, the partitioning of ions in water monolayers may be required for size-dependent bipolar charging in homogeneous materials (as we have discussed above), *too* much water may have detrimental effects on triboelectrification. Indeed, Stern et al. (2019) have shown that the number of discharges in a simulated, oversaturated volcanic granular flow decrease with water content (up to 27 wt%). More recently, Méndez Harper et al. (2020) showed that even smaller amounts of water (below the saturation limit) can reduce the magnitude of triboelectric charging if pyroclasts have high residence times in humid environments. Using a fluidized bed, Toth III et al. (2017) showed that granular materials still charge at high humidities, but that these conditions effectively nullify SDBC (i.e. a large particle is equally likely to be charged negatively as a small particle). Taking these results into consideration, our work suggests that ice-free charging may be extremely efficient at producing charged grains and separating positive and negative particles from each other in relatively dry flows (that is, during the initial, hot phase of an eruption or non-hydromagmatic eruptions). However, the condensation of water may rapidly shut off triboelectric or fractoelectric processes in volcanic columns by reducing both the magnitude of charging and the degree to which charge polarity is separated by size. In this respect, further experimental constraints are needed to better determine the role of water (and other volatiles) on the size-dependent bipolar charging of volcanic materials.

5. Conclusions

We have simulated volcanic jets and proximal electrical phenomena using a shock-tube. To the best of our knowledge, this work demonstrates the presence of size-dependent bipolar charging in a spark-bearing granular flow for the first time. The segregation of charge based on particle size has been associated with triboelectric charging in numerous granular flows over the last 30 years. The detection of SDBC in our experiments, together with investigations at Sakurajima, suggests that frictional electrification may play a significant role in driving electrostatic phenomena within the proximal re-

gion of a volcanic column. Specifically, triboelectrification, through SDBC, can both efficiently electrify pyroclasts and drive charge separation to set up the electric fields needed for the production of lightning. Our analysis, however, does not rule out other synergistic electrification mechanisms such as fractocharging or radioactive decay. In fact, field measurements suggest that triboelectrification alone cannot account for observed charge structures in small volcanic columns. Additionally, we showed that particles emerging from the region where filamentary discharges occur still carry some charge. A first order assessment indicates that particles exiting the gas-thrust region with only a fraction of the theoretical maximum surface charge density would still produce regions with volumetric charge densities capable of sustaining meso-scale lightning. Thus, both vent discharges and larger near-vent lightning may be underpinned by the same electrification mechanisms.

6. Acknowledgments

Joshua Méndez Harper: Conceptualization, Conducted experiments, Hardware, Data Analysis, Writing. Corrado Cimorelli: Conceptualization, Conducted experiments, Reviewing and Editing. Valeria Cigala: Conducted experiments. Ulrich Kueppers: Conducted experiments. Josef Dufek: Conceptualization, Writing- Reviewing, and Editing.

C.C. acknowledges the support of Deutsche Forschungsgemeinschaft project CI 254/2-1. J.M.H and J.D. acknowledge the support of NASA SSW 80NSSC19K1211 and NASA IDS 1911057Z4.

References

- Aizawa, K., Cimorelli, C., Alatorre-Ibarguengoitia, M. A., Yokoo, A., Dingwell, D. B., & Iguchi, M. (2016). Physical properties of volcanic lightning: Constraints from magnetotelluric and video observations at Sakurajima volcano, Japan. *Earth and Planetary Science Letters*, *444*, 45–55. URL: <http://www.sciencedirect.com/science/article/pii/S0012821X1630111X>. doi:10.1016/j.epsl.2016.03.024.
- Aplin, K. L., Houghton, I. M. P., & Nicoll, K. A. (2014). Electrical charging of ash in Icelandic volcanic plumes. *arXiv:1404.6905 [physics]*, . URL: <http://arxiv.org/abs/1404.6905>. ArXiv: 1404.6905.

- Baytekin, H. T., Patashinski, A. Z., Branicki, M., Baytekin, B., Soh, S., & Grzybowski, B. A. (2011). The Mosaic of Surface Charge in Contact Electrification. *Science*, *333*, 308–312. URL: <http://science.sciencemag.org/content/333/6040/308>. doi:10.1126/science.1201512.
- Behnke, S. A., & Bruning, E. C. (2015). Changes to the turbulent kinematics of a volcanic plume inferred from lightning data. *Geophysical Research Letters*, *42*, 2015GL064199. URL: <http://onlinelibrary.wiley.com/doi/10.1002/2015GL064199/abstract>. doi:10.1002/2015GL064199.
- Behnke, S. A., Edens, H. E., Thomas, R. J., Smith, C. M., McNutt, S. R., Van Eaton, A., Cimorelli, C., & Cigala, V. (2018). Investigating the origin of continual radio frequency impulses during explosive volcanic eruptions. *Journal of Geophysical Research: Atmospheres*, *123*, 4157–4174.
- Behnke, S. A., Thomas, R. J., McNutt, S. R., Schneider, D. J., Krehbiel, P. R., Rison, W., & Edens, H. E. (2013). Observations of volcanic lightning during the 2009 eruption of Redoubt Volcano. *Journal of Volcanology and Geothermal Research*, *259*, 214–234. URL: <http://www.sciencedirect.com/science/article/pii/S0377027311003325>. doi:10.1016/j.jvolgeores.2011.12.010.
- Cimorelli, C., Alatorre-Ibarguengoitia, M. A., Aizawa, K., Yokoo, A., Diaz-Marina, A., Iguchi, M., & Dingwell, D. B. (2016). Multiparametric observation of volcanic lightning: Sakurajima Volcano, Japan. *Geophysical Research Letters*, *43*, 2015GL067445. URL: <http://onlinelibrary.wiley.com/doi/10.1002/2015GL067445/abstract>. doi:10.1002/2015GL067445.
- Cimorelli, C., Alatorre-Ibarguengoitia, M. A., Kueppers, U., Scheu, B., & Dingwell, D. B. (2014). Experimental generation of volcanic lightning. *Geology*, *42*, 79–82. URL: <http://geology.gsapubs.org/content/42/1/79>. doi:10.1130/G34802.1.
- Del Bello, E., Taddeucci, J., Vitturi, M. d., Scarlato, P., Andronico, D., Scollo, S., Kueppers, U., & Ricci, T. (2017). Effect of particle volume fraction on the settling velocity of volcanic ash particles: insights from joint experimental and numerical simulations. *Scientific reports*, *7*, 1–11.

- Dickinson, J., Donaldson, E., & Park, M. (1981). The emission of electrons and positive ions from fracture of materials. *Journal of Materials Science*, *16*, 2897–2908.
- Dufek, J., Manga, M., & Patel, A. (2012). Granular disruption during explosive volcanic eruptions. *Nature Geoscience*, *5*, 561–564. URL: <http://www.nature.com/ngeo/journal/v5/n8/abs/ngeo1524.html>. doi:10.1038/ngeo1524.
- Duff, N., & Lacks, D. J. (2008). Particle dynamics simulations of triboelectric charging in granular insulator systems. *Journal of Electrostatics*, *66*, 51–57. URL: <http://www.sciencedirect.com/science/article/pii/S0304388607000952>. doi:10.1016/j.elstat.2007.08.005.
- Dwyer, J. R., & Uman, M. A. (2014). The physics of lightning. *Physics Reports*, *534*, 147–241.
- Forward, K. M., Lacks, D. J., & Sankaran, R. M. (2009). Particle-size dependent bipolar charging of Martian regolith simulant. *Geophysical Research Letters*, *36*, L13201. URL: <http://onlinelibrary.wiley.com/doi/10.1029/2009GL038589/abstract>. doi:10.1029/2009GL038589.
- Gaudin, D., & Cimorelli, C. (2019). The electrification of volcanic jets and controlling parameters: A laboratory study. *Earth and Planetary Science Letters*, *513*, 69–80.
- Gilbert, J. S., Lane, S. J., Sparks, R. S. J., & Koyaguchi, T. (1991). Charge measurements on particle fallout from a volcanic plume. *Nature*, *349*, 598–600. URL: <http://www.nature.com/nature/journal/v349/n6310/abs/349598a0.html>. doi:10.1038/349598a0.
- Gu, Z., Wei, W., Su, J., & Yu, C. W. (2013). The role of water content in triboelectric charging of wind-blown sand. *Scientific Reports*, *3*, 1337. URL: <http://www.nature.com/srep/2013/130225/srep01337/full/srep01337.html>. doi:10.1038/srep01337.
- Harrison, R. G., Barth, E., Esposito, F., Merrison, J., Montmessin, F., Aplin, K. L., Borlina, C., Berthelier, J.-J., Déprez, G., Farrell, W. M. et al. (2016). Applications of electrified dust and dust devil electrostatics to martian atmospheric electricity. *Space Science Reviews*, *203*, 299–345.

- Hatakeyama, H., & Uchikawa, K. (1951). On the disturbance of the atmospheric potential gradient caused by the eruption-smoke of the volcano aso. *Papers in Meteorology and Geophysics*, *2*, 85–89.
- James, M., Lane, S., & Gilbert, J. S. (2000). Volcanic plume electrification: Experimental investigation of a fracture-charging mechanism. *Journal of Geophysical Research: Solid Earth*, *105*, 16641–16649.
- Kikuchi, K., & Endoh, T. (1982). Atmospheric electrical properties of volcanic ash particles in the eruption of Mt. Usu Volcano, 1977. *Journal of the Meteorological Society of Japan*, *1*, 548–561.
- Lacks, D. J., & Levandovsky, A. (2007). Effect of particle size distribution on the polarity of triboelectric charging in granular insulator systems. *Journal of Electrostatics*, *65*, 107–112. URL: <http://www.sciencedirect.com/science/article/pii/S0304388606000866>. doi:10.1016/j.elstat.2006.07.010.
- Lacks, D. J., & Sankaran, R. M. (2011). Contact electrification of insulating materials. *Journal of Physics D: Applied Physics*, *44*, 453001. URL: <http://stacks.iop.org/0022-3727/44/i=45/a=453001>. doi:10.1088/0022-3727/44/45/453001.
- Lacks, D. J., & Shinbrot, T. (2019). Long-standing and unresolved issues in triboelectric charging. *Nature Reviews Chemistry*, *3*, 465–476.
- Méndez Harper, J., & Dufek, J. (2016). The effects of dynamics on the triboelectrification of volcanic ash. *Journal of Geophysical Research: Atmospheres*, (p. 2015JD024275). URL: <http://onlinelibrary.wiley.com/doi/10.1002/2015JD024275/abstract>. doi:10.1002/2015JD024275.
- Méndez Harper, J., McDonald, G., Dufek, J., Malaska, M., Burr, D., Hayes, A., McAdams, J., & Wray, J. (2017). Electrification of sand on titan and its influence on sediment transport. *Nature Geoscience*, *10*, 260–265. URL: <https://doi.org/10.1038/ngeo2921>. doi:10.1038/ngeo2921.
- Méndez Harper, J., Cimarelli, C., Dufek, J., Gaudin, D., & Thomas, R. J. (2018a). Inferring compressible fluid dynamics from vent discharges during volcanic eruptions. *Geophys. Res. Lett.*, *45*, 7226–7235. URL: <https://doi.org/10.1029/2018GL078286> doi:10.1029/2018GL078286.

- Méndez Harper, J., Helling, C., & Dufek, J. (2018b). Triboelectrification of kcl and zns particles in approximated exoplanet environments. *The Astrophysical Journal*, *867*, 123. URL: <https://doi.org/10.3847/1538-4357/aadf36>. doi:10.3847/1538-4357/aadf36.
- Méndez Harper, J., Steffes, P., Dufek, J., & Akins, A. (2019). The effect of electrostatic charge on the propagation of gps (l-band) signals through volcanic plumes. *Journal of Geophysical Research: Atmospheres*, *124*, 2260–2275. URL: <https://doi.org/10.1029/2018JD029076>. doi:10.1029/2018JD029076.
- Méndez Harper, J., Courtland, L., Dufek, J., & McAdams, J. (2020). Microphysical effects of water content and temperature on the triboelectrification of volcanic ash on long timescales. *Journal of Geophysical Research: Atmospheres*, *125*, e2019JD031498. URL: <https://doi.org/10.1029/2019JD031498>. doi:10.1029/2019JD031498.
- Méndez Harper, J., Dufek, J., & McDonald, G. D. (2021). Detection of spark discharges in an agitated mars dust simulant isolated from foreign surfaces. *Icarus*, *357*, 114268. <https://doi.org/10.1016/j.icarus.2020.114268> doi:10.1029/10.1016/j.icarus.2020.114268.
- Miura, T., Koyaguchi, T., & Tanaka, Y. (2002). Measurements of electric charge distribution in volcanic plumes at sakurajima volcano, japan. *Bulletin of volcanology*, *64*, 75–93.
- Nicoll, K., Airey, M., Cimarelli, C., Bennett, A., Harrison, G., Gaudin, D., Aplin, K., Koh, K. L., Knuever, M., & Marltton, G. (2019). First in situ observations of gaseous volcanic plume electrification. *Geophysical Research Letters*, *46*, 3532–3539.
- Pahtz, T., Herrmann, H. J., & Shinbrot, T. (2010). Why do particle clouds generate electric charges? *Nature Physics*, *6*, 364–368. URL: <http://www.nature.com/nphys/journal/v6/n5/abs/nphys1631.html>. doi:10.1038/nphys1631.
- Pan, S., & Zhang, Z. (2019). Fundamental theories and basic principles of triboelectric effect: A review. *Friction*, *7*, 2–17.

- Petersen, D., Bailey, M., Beasley, W. H., & Hallett, J. (2008). A brief review of the problem of lightning initiation and a hypothesis of initial lightning leader formation. *Journal of Geophysical Research: Atmospheres*, *113*.
- Prata, A., Folch, A., Prata, A., Biondi, R., Brenot, H., Cimarelli, C., Corradini, S., Lapierre, J., & Costa, A. (2020). Anak Krakatau triggers volcanic freezer in the upper troposphere. *Scientific reports*, *10*, 1–13.
- Smith, C. M., Van Eaton, A. R., Charbonnier, S., McNutt, S. R., Behnke, S. A., Thomas, R. J., Edens, H. E., & Thompson, G. (2018). Correlating the electrification of volcanic plumes with ashfall textures at sakurajima volcano, Japan. *Earth and Planetary Science Letters*, *492*, 47–58.
- Smith, C. M., Thompson, G., Reader, S., Behnke, S. A., McNutt, S. R., Thomas, R., & Edens, H. (2020). Examining the statistical relationships between volcanic seismic, infrasound, and electrical signals: A case study of sakurajima volcano, 2015. *Journal of Volcanology and Geothermal Research*, *402*, 106996.
- Stern, S., Cimarelli, C., Gaudin, D., Scheu, B., & Dingwell, D. (2019). Electrification of experimental volcanic jets with varying water content and temperature. *Geophysical Research Letters*, *46*, 11136–11145.
- Suzuki, Y., Costa, A., Cerminara, M., Ongaro, T. E., Herzog, M., Van Eaton, A. R., & Denby, L. (2016). Inter-comparison of three-dimensional models of volcanic plumes. *Journal of Volcanology and Geothermal Research*, *326*, 26–42.
- Takahashi, T. (2012). Precipitation particle charge distribution and evolution of east Asian rainbands. *Atmospheric research*, *118*, 304–323.
- Thomas, R. J., Krehbiel, P. R., Rison, W., Edens, H. E., Aulich, G. D., Winn, W. P., McNutt, S. R., Tytgat, G., & Clark, E. (2007). Electrical Activity During the 2006 Mount St. Augustine Volcanic Eruptions. *Science*, *315*, 1097–1097. URL: <http://science.sciencemag.org/content/315/5815/1097>. doi:10.1126/science.1136091.
- Toth III, J. R., Phillips, A. K., Rajupet, S., Sankaran, R. M., & Lacks, D. J. (2017). Particle-size-dependent triboelectric charging in single-component granular materials: role of humidity. *Industrial & Engineering Chemistry Research*, *56*, 9839–9845.

- Van Eaton, A. R., Schneider, D. J., Smith, C. M., Haney, M. M., Lyons, J. J., Said, R., Fee, D., Holzworth, R. H., & Mastin, L. G. (2020). Did ice-charging generate volcanic lightning during the 2016–2017 eruption of bogoslof volcano, alaska? *Bulletin of Volcanology*, *82*, 24.
- Vossen, C. E., Cimorelli, C., Bennett, A. J., Geisler, A., Gaudin, D., Miki, D., Iguchi, M., & Dingwell, D. B. (2021). Long-term observation of electrical discharges during persistent vulcanian activity. *Earth and Planetary Science Letters*, *570*, 117084.
- Waitukaitis, S. R., Lee, V., Pierson, J. M., Forman, S. L., & Jaeger, H. M. (2014). Size-dependent same-material tribocharging in insulating grains. *Physical Review Letters*, *112*, 218001.
- Wurm, G., Schmidt, L., Steinpilz, T., Boden, L., & Teiser, J. (2019). A challenge for martian lightning: Limits of collisional charging at low pressure. *Icarus*, *331*, 103–109.
- Xie, Y., & Li, Z. (2018). Triboluminescence: recalling interest and new aspects. *Chem*, *4*, 943–971.
- Zhao, H., Castle, G. P., Inculet, I. I., & Bailey, A. G. (2003). Bipolar charging of poly-disperse polymer powders in fluidized beds. *IEEE Transactions on Industry Applications*, *39*, 612–618.